All-Solid-State Nanosecond Pulse Power Supply Based on BLTs and Pulse Transformer for DBD Application

Hao Gui, Zhongyong Zhao, *Member, IEEE*, Qing Shi, Xin Liu, *Student Member, IEEE*, and Chenguo Yao, *Member, IEEE*

***Abstract*—Nanosecond(ns) pulses have been proven to drive dielectric barrier discharge (DBD) more efficiently. However, the DBD device is a capacitive load, which will cause distortions in the pulse waveform of the power supply. To maintain the ns pulse waveform, a parallel resistor is normally set to overcome the influence of DBD loads in the traditional methods, which will cause extra energy loss. This article proposed a bipolar ns pulse power supply for DBD based on Blumlein transmission lines and pulse transformer. It does not need to set a parallel resistor and can adapt well to the load characteristics of DBD. This topology can output bipolar ns pulses on DBD loads with a rise time of 100 ns, a pulsewidth of 300 ns, an adjustable amplitude of 0–5 kV, and a maximum repetition frequency of 20 kHz. In this context, the operating characteristics of the circuit are derived based on the lossless transmission line model and Laplace transform, and then the correctness of the theoretical derivation is verified by the prototype. The results showed that the proposed ns power supply can drive DBD loads with adjustable output voltage amplitude and frequency.**

***Index Terms*—Bipolar nanosecond pulse, Blumlein transmission lines (BLTs), dielectric barrier discharge (DBD), pulse transformer, pulsed power technology, solid-state switches.**

I. Introduction

DIELECTRIC barrier discharge (DBD) has attracted extensive attention because it can produce a large number of active particles at low temperatures and atmospheric pressure. At present, DBD technology has been widely used in material surface treatment [1], [2], [3], [4], waste gas and sewage purification [5], [6], [7], ozone synthesis and UV generation [8], [9], and biomedicine [10], [11].

Now, the excitation power sources used to generate DBD could be mainly divided into three types: high-frequency high-voltage ac power sources [8], [12], [13], microsecond pulse power sources [14], [15], [16], and nanosecond(ns) pulse power sources [17], [18], [19], [20], among which researchers follow with interest in nanosecond pulse power sources due to their characteristics of short discharge time and steep rising and falling edges, which are conducive to the formation of uniform and stable discharge [21], [22]. Obtaining stable DBD plasma in millimeter gaps requires not only pulse amplitudes reaching thousands of volts but also pulse repetition frequency reaching high frequencies. Thus, solid-state switches have been widely used in ns pulse power supplies due to their superior performance [23]. Rao et al. [16] fabricated an ns pulse power supply based on the magnetic switches, combined with the Marx structure and BTLs for DBD with a maximum output amplitude of 20 kV and pulsewidth of 220 ns. However, the output waveform oscillated severely due to the mismatch of impedance. In [17], an ns pulse power supply based on the magnetic compression structure with a maximum amplitude of 30 kV and a pulsewidth of 70 ns suitable for DBD was proposed, but the maximum repetition frequency of the output pulse was only 1 kHz due to the performance of the magnetic switch. Mi et al. [18] obtained an ns pulse power supply suitable for DBD with a maximum repetition frequency of 10 kHz and a maximum amplitude of 13 kV by improving the performance of the magnetic switch. Dhakar et al. [20] used a wide bandgap device instead of magnetic compression on the primary side, which improved the repetition frequency of the power supply.

However, since the DBD device is a capacitive load, many topologies designed compensation circuits to adapt the load characteristics of DBD. Bonnin et al. [12] and Hao et al. [13] designed compensation circuits to improve the energy consumption on the load side of DBD. Usually, to maintain the ns pulse waveform, a parallel resistor is set to overcome the influence of DBD loads. Shao et al. [17], [18], [19], [20] and Wang et al. [25] used parallel resistors with different resistance values to

Manuscript received 11 August 2022; revised 20 December 2022; accepted 28 April 2023. Date of publication 9 May 2023; date of current version 21 June 2023. This work was supported in part by Sichuan Science and Technology Program under Grant 2023NSFSC0829, in part by the Fundamental Research Funds for the Central Universities under Grant SWU-KT22027, and in part by the Venture and Innovation Support Program for Chongqing Overseas Returnees under Grant cx2019123. Recommended for publication by Associate Editor F. COSTA. *(Corresponding author: Zhongyong Zhao.)*

Hao Gui and Qing Shi are with the College of Engineering and Technology, Southwest University, Chongqing 400716, China, and also with the Yibin Academy of Southwest University, Yibin 644000, China (e-mail: gh5261657@email.swu.edu.cn; sq12345@email.swu.edu.cn).

Zhongyong Zhao is with the College of Engineering and Technology, Southwest University, Chongqing 400716, China, also with the Yibin Academy of Southwest University, Yibin 644000, China, and also with the Jinfeng Laboratory, Chongqing 401329, China (e-mail: zhaozy1988@swu.edu.cn).

Xin Liu is with the School of Electrical Engineering, Chongqing University, Chongqing 400044, China (e-mail: alxenderking@cqu.edu.cn).

Chenguo Yao is with the School of Electrical Engineering, Chongqing University, Chongqing 400044, China, and also with Jinfeng Laboratory, Chongqing 401329, China (e-mail: yaochenguo@cqu.edu.cn).

Color versions of one or more figures in this article are available at https://doi.org/10.1109/TPEL.2023.3274451.

Digital Object Identifier 10.1109/TPEL.2023.3274451

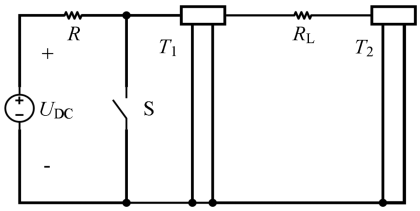

Fig. 1. Typical circuit diagram of BLTs, which mainly consist of a DC power supply, control switch S, charge resistor R, two transmission lines T_1 and T_2, and load R_L.

maintain the ns pulse. Although a parallel resistor is helpful to retain the pulse ns waveform, it will also cause extra energy loss, which may be much larger than the energy consumed by the DBD loads.

To avoid extra energy consumption on the parallel resistor and improve the energy utilization of ns pulse topologies for driving the DBD loads, this article proposes a structure that combines the BTLs with a step-up pulse transformer. It can produce high-voltage bipolar ns pulses on the DBD load without the parallel resistor and has the advantages of Blumlein transmission lines (BLTs) and solid-state switches: compact structure, simple controllability, and good stability. Combined with a pulse transformer, it can adapt well to the load characteristics of DBD and overcome the disadvantages of the conventional BLT structures that can hardly maintain high pulse amplitude and high repetition frequency simultaneously. This power supply can output ns pulses with a rise time of 100 ns, a pulsewidth of 300 ns, an adjustable amplitude of 0–5 kV, and a maximum repetition frequency of 20 kHz.

The rest of this article is organized as follows. Section II explains the effectiveness of the proposed power supply topology based on the transmission line theory and Laplace transform. Section III studies the specific production process of power supply, including the production of BLTs and pulse transformer. Then, the DBD experiments based on the proposed power supply are carried out and the results are discussed in Section IV. Finally, Section V concludes this article.

II. Schematic Analysis of the Circuit Topology

A typical circuit of BLTs has shown in Fig. 1. The basic operating principle is as follows: First, the high-voltage dc power supply charges the transmission lines T_1 and T_2 to the desired charging voltage through the current limiting resistor R. Then, the control switch S is closed to form a fold reflection of the voltage wave on the load R_L. Assume that the impedance of transmission is Z and the amplitude of U_{DC} is 1 V when the impedance of load R_L changes from 3.5 to 0.5Z, and the voltage waves on the load R_L are shown in Fig. 2.

It can be seen that when the load impedance equal 2Z, a square-wave pulse with a pulsewidth twice the propagation time will be produced on the load. In contrast, when the load impedance does not equal to 2Z, the voltage wave will oscillate obviously.

Now, consider the structure of BLTs combined with a pulse transformer and a DBD load, as shown in Fig. 3, in which

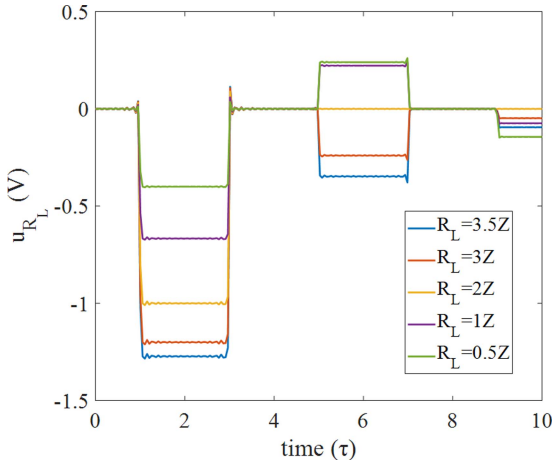

Fig. 2. Voltage waves on the load R_L when its impedance changes from 3.5 to 0.5Z, where τ means the propagation time of transmission.

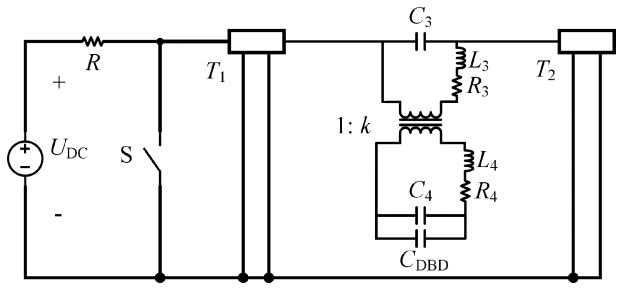

Fig. 3. Circuit topology of BLTs combined with a pulse transformer and a DBD load.

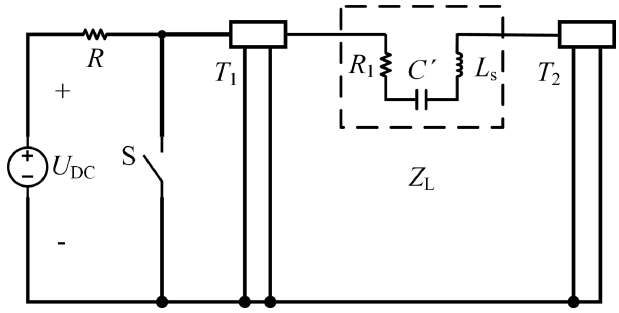

Fig. 4. Circuit topology of the proposed pulse power supply in which the secondary side of the pulse transformer is converted to the primary side.

the parasitic capacitance between the primary and secondary windings is ignored.

In Fig. 3, C_3 and L_3 are the stray capacitance and leakage inductance at the primary side; R_3 is the winding resistance at the primary side; C_4 and L_4 are the stray capacitance and leakage inductance at the secondary side; R_4 is the winding resistance at the secondary side; the transformation ratio of pulse transformer is 1: k and C_{DBD} is the load at the secondary side of the pulse transformer.

The parameters of the secondary side are converted to the primary side, and the stray capacitance and winding resistance of the primary side are ignored [24]. The equivalent circuit is shown in Fig. 4.

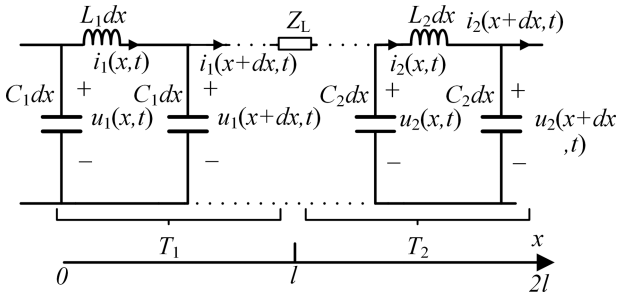

Fig. 5. Equivalent circuit diagram of lossless transmission line of BLTs after charging, where i_1, i_2, u_1, and u_2 are the currents and voltages on transmission lines T_1 and T_2, respectively, and L_1, C_1, L_2, and C_2 are the distributed inductance and distributed capacitance of the two transmission lines, respectively. And U_{DC} is the charge voltage of transmission lines.

In Fig. 4, there are

$$\begin{cases} C' = k^2(C_{\mathrm{DBD}} + C_4) \\ L_S = L_3 + \frac{1}{k^2}L_4 \\ R_1 = R_3 + \frac{1}{k^2}R_4 \\ Z_L = R_1 + sL_s + \frac{1}{sC'}. \end{cases} \tag{1}$$

When the charging of the transmission line is completed and the switch S is closed, the equivalent circuit diagram of the lossless transmission line of BLTs is shown in Fig. 5.

The telegraph equation of transmission lines is

$$\begin{cases} L_1\frac{\partial i_1}{\partial t} + \frac{\partial u_1}{\partial x} = 0 \\ \frac{\partial i_1}{\partial x} + C_1\frac{\partial u_1}{\partial t} = C_1U_{\mathrm{DC}} \\ L_2\frac{\partial i_2}{\partial t} + \frac{\partial u_2}{\partial x} = 0 \\ \frac{\partial i_2}{\partial x} + C_2\frac{\partial u_2}{\partial t} = C_2U_{\mathrm{DC}}. \end{cases} \tag{2}$$

The above equations are transformed to the Laplace domain

$$\begin{cases} sL_1I_1 + \frac{\partial U_1}{\partial x} = 0 \\ \frac{\partial I_1}{\partial x} + sC_1U_1 = C_1U_{\mathrm{DC}} \\ sL_2I_2 + \frac{\partial U_2}{\partial x} = 0 \\ \frac{\partial I_2}{\partial x} + sC_2U_2 = C_2U_{\mathrm{DC}} \end{cases} \tag{3}$$

where s is the Laplace variable. Also, there are boundary conditions

$$\begin{cases} U_1(0,s) = 0 \\ U_1(l,s) - U_2(l,s) = Z_LI_1(l,s) \\ I_1(l,s) = I_2(l,s) \\ I_2(2l,s) = 0. \end{cases} \tag{4}$$

Now, consider the transmission line as an equilibrium state

$$\begin{cases} Z_1 = \sqrt{\frac{L_1}{C_1}} = Z_2 = \sqrt{\frac{L_2}{C_2}} = Z \\ v_1 = \frac{1}{\sqrt{L_1C_1}} = v_2 = \frac{1}{\sqrt{L_2C_2}} = v \end{cases} \tag{5}$$

where Z_1 and Z_2 are the characteristic impedances of the transmission lines T_1 and T_2, respectively. v_1 and v_2 are the propagation speeds of the voltage wave in the transmission lines.

The general solution of the equation is obtained as follows:

$$\begin{cases} U_1 = A_1e^{\frac{x}{v}s} + B_1e^{\frac{-x}{v}s} + \frac{U_{\mathrm{DC}}}{s} \\ I_1 = \frac{1}{Z}(A_1e^{\frac{x}{v}s} - B_1e^{\frac{-x}{v}s}) \\ U_2 = A_2e^{\frac{x}{v}s} + B_2e^{\frac{-x}{v}s} + \frac{U_{\mathrm{DC}}}{s} \\ I_2 = \frac{1}{Z}(A_2e^{\frac{x}{v}s} - B_2e^{\frac{-x}{v}s}). \end{cases} \tag{6}$$

Bringing in the boundary conditions, we have

$$\begin{cases} A_1 + B_1 = -\frac{U_{\mathrm{DC}}}{s} \\ A_1e^{\frac{x}{v}s} - B_1e^{\frac{-x}{v}s} = A_2e^{\frac{x}{v}s} - B_2e^{\frac{-x}{v}s} \\ A_2e^{\frac{4x}{v}s} = B_2 \\ \left[\left(\frac{Z_L}{Z}+1\right)A_1 - A_2\right]e^{\frac{x}{v}s} = [(\frac{Z_L}{Z}-1)B_1 + B_2]e^{\frac{-x}{v}s}. \end{cases} \tag{7}$$

Let

$$\tau = \frac{l}{v}. \tag{8}$$

The solution gives

$$\begin{cases} I_2(s,l) = \frac{1}{Z}\cdot\frac{2U_{\mathrm{DC}}}{s}\cdot\left[\frac{e^{\frac{3l}{v}s} - e^{\frac{l}{v}s}}{(\frac{Z_L}{Z}+2)e^{\frac{4l}{v}s} + 2 - \frac{Z_L}{Z}}\right] \\ U_{Z_L} = -\frac{Z_L}{Z}\cdot\frac{2U_{\mathrm{DC}}}{s}\cdot\left[\frac{e^{\frac{3l}{v}s} - e^{\frac{l}{v}s}}{(\frac{Z_L}{Z}+2)e^{\frac{4l}{v}s} + 2 - \frac{Z_L}{Z}}\right]. \end{cases} \tag{9}$$

For the load, there are

$$\begin{aligned} U_{C'} &= -\frac{1}{sC'}\cdot\frac{1}{Z}\cdot\frac{2U_{\mathrm{DC}}}{s}\cdot\left[\frac{e^{3\tau s} - e^{\tau s}}{(\frac{Z_L}{Z}+2)e^{4\tau s} + 2 - \frac{Z_L}{Z}}\right] \\ &= -\frac{2U_{\mathrm{DC}}}{s}\cdot\left[\frac{e^{3\tau s} - e^{\tau s}}{(R_1C'+L_sC's^2+1)(e^{4\tau s}-1) + 2ZC'(e^{4\tau s}+1)}\right]. \end{aligned} \tag{10}$$

Then, the voltage on the DBD load is obtained as follows:

$$\begin{aligned} U_{C_{\mathrm{DBD}}} &= k\cdot U_{C'} \\ &= -k\cdot\frac{2U_{\mathrm{DC}}}{s}\cdot\left[\frac{e^{3\tau s} - e^{\tau s}}{(R_1C'+L_sC's^2+1)(e^{4\tau s}-1) + 2ZC'(e^{4\tau s}+1)}\right]. \end{aligned} \tag{11}$$

Let

$$\begin{cases} a = k^2L_s(C_4 + C_{\mathrm{DBD}}) \\ b = k^2R_1(C_4 + C_{\mathrm{DBD}}) \\ c = 2k^2Z(C_4 + C_{\mathrm{DBD}}). \end{cases} \tag{12}$$

It is obtained that

$$U_{C_{\mathrm{DBD}}} = -k\cdot\frac{2U_{\mathrm{DC}}}{s}\cdot\frac{e^{3\tau s} - e^{\tau s}}{(as^2+bs+1)(e^{4\tau s}-1) + c(e^{4\tau s}+1)}. \tag{13}$$

In the ideal case, the stray capacitance as well as the leakage inductance of the pulse transformer are very small, while in general, the load C_{DBD} is a small capacitance of pF level, so the above formula can be approximated as follows:

$$\begin{aligned} U_{C_{\mathrm{DBD}}} &\approx -k\cdot\frac{2U_{\mathrm{DC}}}{s}\cdot\left[\frac{e^{3\tau s} - e^{\tau s}}{e^{4\tau s}-1}\right] \\ &= -k\cdot\frac{2U_{\mathrm{DC}}}{s}\cdot(e^{3\tau s} - e^{\tau s})\cdot\frac{1}{e^{4\tau s}-1} \\ &= -k\cdot\frac{2U_{\mathrm{DC}}}{s}\cdot(e^{3\tau s} - e^{\tau s})\cdot\sum_{n=1}^{\infty}e^{-4n\tau s}. \end{aligned} \tag{14}$$

Transform the above formula to the time domain

$$u_{C_{\mathrm{DBD}}} = -2kU_{\mathrm{DC}}\cdot\sum_{n=1}^{\infty}\sigma[t + (3-4n)\tau] - \sigma[t + (1-4n)\tau] \tag{15}$$

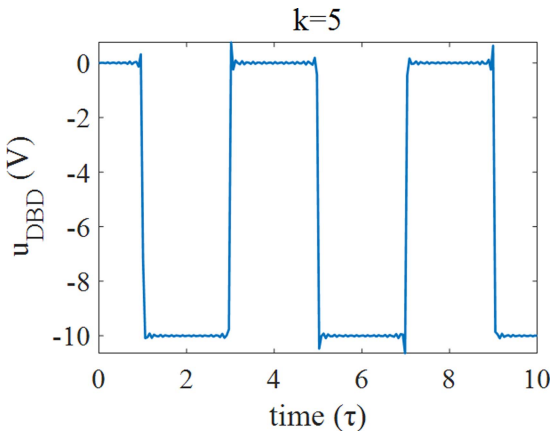

Fig. 6. Theoretical DBD load voltage waveform when the step-up ratio is 1:5 before gas discharge and assume the amplitude of U_{DC} is 1 V.

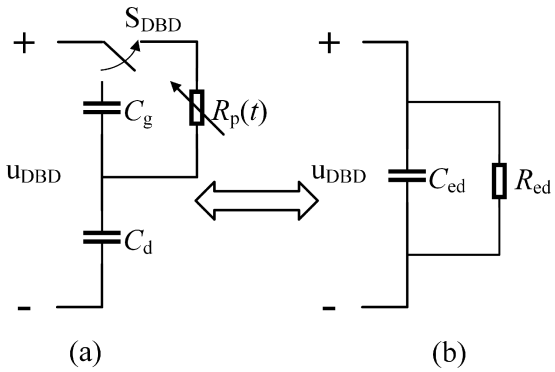

Fig. 7. Equivalent model of DBD load, where C_g is the capacitance of gas and C_d is the dielectric capacitance. The switch S_{DBD} is closed when gas discharge happens and circuit (a) can be converted to circuit (b) in [25].

where $\sigma(t)$ represents the step function. And the time-domain waveform at the load side is shown in Fig. 6.

Based on the above derivation, when the loss on the line is not considered, it is clear that before the gas discharge, the topology of Fig. 3 will produce a periodic unipolar pulse with a pulsewidth of 2τ and amplitude of $2k$ times the charging voltage on the DBD load. Ideally, the DBD load can be equivalent to an infinite resistance based on the formula (9)–(11) before discharge.

In the actual case, the DBD load can be equivalent to the circuit of Fig. 7 [25], the switch S_{DBD} is closed when the gas discharge occurs, and the load is a time-varying plasma resistor $R_p(t)$ and series capacitor C_d.

To simplify circuit analysis, the DBD load is equivalent to a resistor in parallel with a capacitor, as illustrated in Fig. 7(b).

Then, we have

$$Z_L = R_1 + sL_S + \frac{\frac{1}{sC_4}\|(R_{ed}\|\frac{1}{sC_{ed}})}{k^2} \tag{16}$$

$$U_{Z_L} = \frac{Z_L}{Z}\cdot\frac{2U_{DC}}{s}\cdot\left[\frac{e^{3\tau s}-e^{\tau s}}{(\frac{Z_L}{Z}+2)e^{4\tau s}+2-\frac{Z_L}{Z}}\right] \tag{17}$$

$$U_{DBD} = U_{Z_L}\cdot\frac{\frac{1}{sC_4}\|(R_{ed}\|\frac{1}{sC_{ed}})}{k^2\cdot Z_L}\cdot k. \tag{18}$$

TABLE I
VALUES OF PARAMETERS IN FORMULA (18)

Name of parameter	Value
The characteristic impedance of transmission line Z/Ω	50
The stray capacitance C_4/pF	10
The leakage inductance L_s/μH	2
The winding resistance R_1/Ω	5
Discharge equivalent capacitance C_{ed}/pF	40
Discharge equivalent resistance R_{ed}/Ω	1000

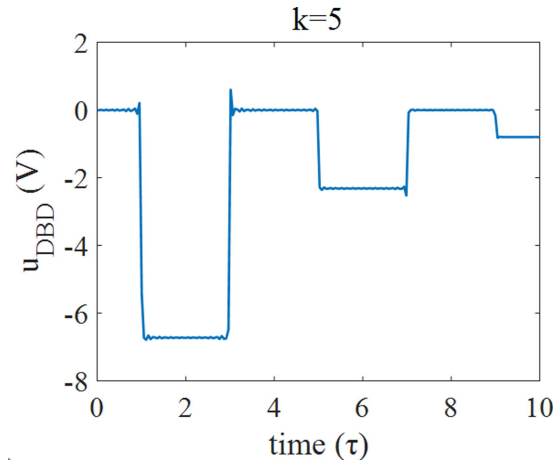

Fig. 8. Theoretical DBD load voltage waveform when gas discharge occurs. Assume the amplitude of U_{DC} is 1 V.

Assume that the values of parameters in the transmission lines and pulse transformer and DBD load are shown in Table I.

Since the function U_{DBD} does not have an analytic expression in the time domain, its time-domain waveform is calculated by numerical integration, and from the Laplace inverse transform, we have

$$\begin{aligned} u_{C_{DBD}} &= \frac{1}{j2\pi}\int_{\sigma-j\infty}^{\sigma+j\infty} U_{C_{DBD}}(s,l)\cdot e^{st}ds \\ &= \frac{e^{\sigma t}}{2\pi}\int_{-\infty}^{+\infty} U_{C_{DBD}}(s,l)\cdot e^{j\omega t}d\omega \\ &= \frac{e^{\sigma t}}{2\pi}\int_{-\infty}^{+\infty} U_{C_{DBD}}(j\omega+\sigma,l)\cdot e^{j\omega t}d\omega. \end{aligned} \tag{19}$$

And its time-domain waveform is calculated, as shown in Fig. 8.

It can be seen from Fig. 8 that the actual discharge waveform amplitude is lower than the amplitude before discharge, and the load waveform will no longer be an equal-amplitude oscillating pulse but an oscillating decay pulse.

Based on the above analysis, the following points are proved.

1) The topology proposed in this article can obtain a high-voltage pulse with a pulsewidth of 2τ on the DBD load to drive DBDs.
2) The amplitude of the ns pulse is influenced by the DBD load. When the value of plasma resistor $R_p(t)$ is very high, the amplitude is close to $2k$ times the dc charge voltage. When the resistance of plasma becomes small, the amplitude will become lower than $2k$ times the dc charge voltage.

Besides, it has already been proven that if the DBD is driven by a bipolar pulse, the discharge intensity will be significantly larger than that driven by a unipolar pulse. This is because the charge

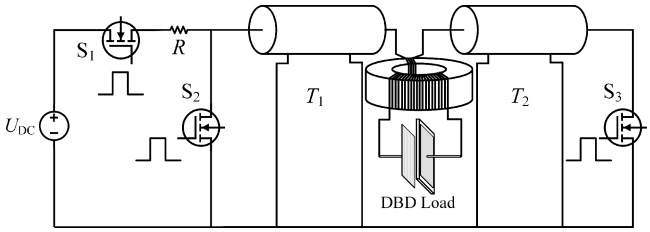

Fig. 9. Overall structure diagram of the proposed power supply in this context.

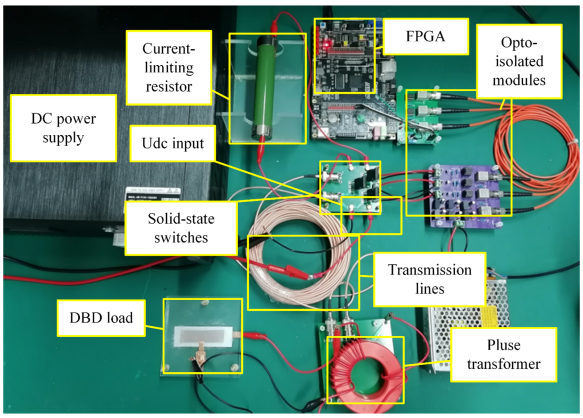

Fig. 10. Actual structure diagram of DBD load connected by the pulse power supply.

accumulation after the previous discharge can reduce the electric field intensity of the second discharge of opposite polarity [26]. Using two switches on the two ends of the transmission lines can generate a bipolar voltage pulse due to the reflection principle of the voltage wave. Therefore, a bipolar ns pulse power supply for DBD by combining the BLTs with a pulse transformer will be designed and manufactured in this study.

III. Design and Manufacture of Pulse Power Supply

Fig. 9 shows the structure of the pulse power supply.

The principle of the pulse power supply is given as follows. First, the field programmable gate array (FPGA) generates the original control signals. It propagates through the optoisolator and driving circuit to produce the charging signal to control the opening of the charging MOSFET S_1. Then, the high-voltage dc power supply charges the BLTs through the noninductive current limiting resistor R. When the charging is completed, the charging signal is withdrawn, and then the discharging signal is generated to control the discharging MOSFETs S_2, S_3, and the BLTs are discharged through the pulse transformer to drive the DBD load.

The image of the pulse power supply is shown in Fig. 10, and it is mainly divided into two parts: the BLTs and the pulse transformer. BLTs mainly consist of transmission lines T_1 and T_2, MOSFETs, and noninductive current limiting resistor R, which is used to protect the dc power supply. When S_2 is turned ON, a negative polarity pulse will be generated on the load R_L. When S_3 is turned ON, a positive polarity pulse will be generated on the load R_L. The electrical parameters of the main components of the BLTs are given in Table II.

TABLE II
Electrical Parameters of the Main Components

Name of parameter	Value
High-voltage DC power supply U_{DC}/V	0–1000
Current-limiting resistor R/Ω	1000
The characteristic impedance of transmission line Z/Ω	50
Withstand voltage of transmission line U/V	1500
Length of transmission L/M	30
Withstand voltage of MOSFET U_M/V	1200

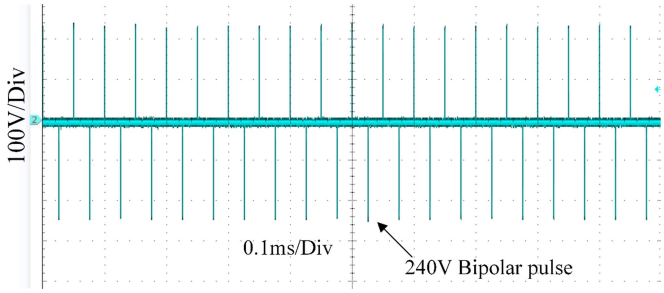

Fig. 11. Collected voltage waveform of the 100 Ω noninductive resistor load connected by the BLTs.

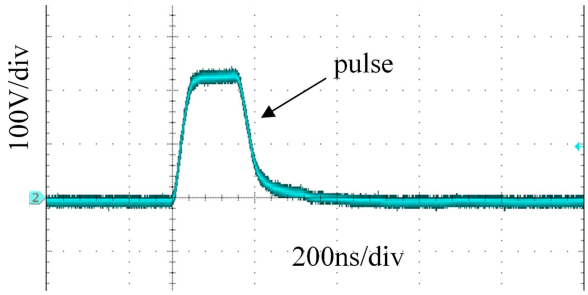

Fig. 12. Collected single-voltage waveform of the 100 Ω noninductive resistor connected by the BLTs.

At a dc charging voltage of 250 V and a repetition of 10 kHz, the continuous bipolar pulse on the 100 Ω noninductive resistor load is measured, as shown in Fig. 11.

The single pulse waveform is shown in Fig. 12, with a pulsewidth of 300 ns, an amplitude of 240 V, and a rising edge of 40 ns. Under a purely resistive load, bipolar pulses of different amplitudes and frequencies can be obtained by adjusting the operating timing of the semiconductor switches in the BLTs and the charging voltage.

It can be seen that the pulse amplitude output by only BLTs is not enough to drive DBD loads. Therefore, based on the analysis in Section II, to drive the DBD, a pulse transformer is required.

Currently, pulse transformers are mainly used in gas pedals, radars, and high-energy physics [27], [28], [29], [30], [31]. The performance of the pulse transformer is mainly determined by the pulsewidth and rise time [24].

For pulse transformers, there are

$$e_1 = N_1 \frac{d\varphi}{dt} \approx N_1 \frac{\Delta\varphi}{\Delta t} = N_1 \frac{\Delta B_{\max} S K_C}{t_{\text{width}}} = U_{\text{in}} \qquad (20)$$

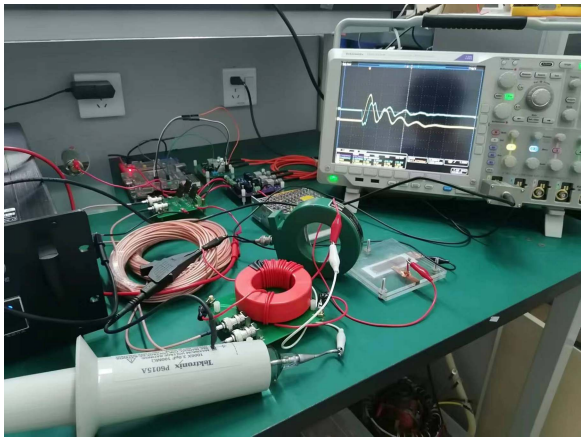

Fig. 13. Experimental platform of DBD.

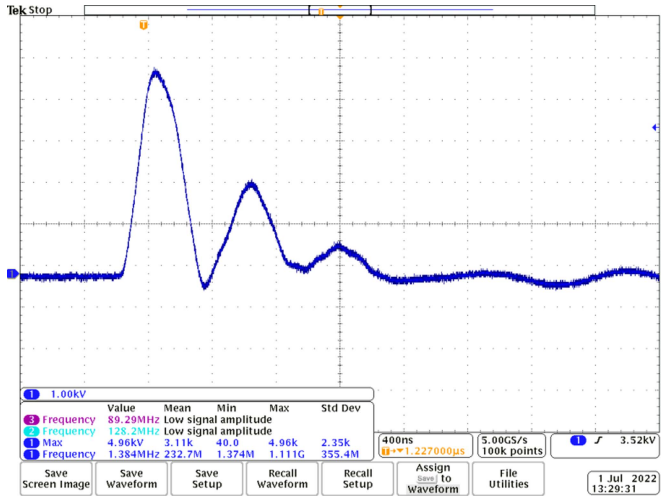

Fig. 14. Maximum output voltage waveform of power supply in this article. The voltage scale is 1 kV/Div., and the timescale is 400 ns/Div.

where φ represents the magnetic flux of the coil per turn, N_1 represents the number of turns of the primary-side winding, t_{width} represents the pulsewidth of the pulse transformer, and $\Delta B_{\max}$ is the maximum induction increment, which equals the difference between the saturated magnetic induction intensity and the rest magnetic induction intensity of the pulse transformer core. K_C represents the duty cycle coefficient of the core, S represents the cross-sectional area of the core, and U_{in} represents the voltage on the primary side of the pulse transformer.

The number of turns of winding N_1 and N_2, and the cross-sectional area of the core S influences the leakage inductance and distributed capacitance. To get a fast rise time of the pulse on DBD load, it is necessary to reduce the leakage inductance and distributed capacitance of the pulse transformer.

Increasing the magnetic permeability of the core can achieve a larger magnetization inductance, thus reducing the number of turns while maintaining the same winding inductance. Besides, a larger $\Delta B_{\max}$ also helps to reduce the core cross-sectional area S, thus reducing the leakage inductance and distributed capacitance, to shorten the pulse rise time.

Based on the analysis above, the nanocrystalline core is selected, which has a saturated magnetic induction of 1.25 T and a rest magnetic induction of 0.2 T, with K_C of 0.77. Compared with the conventional core material, the nanocrystalline core has a larger saturated magnetic induction, a smaller rest magnetic induction, and high efficiency of energy transfer. The final homemade pulse transformer of this study has a primary winding of 3 turns, a secondary winding of 15 turns, and a 1:5 ratio. According to the calculation of the empirical formula, the equivalent leakage inductance obtained from the primary side is 0.126 μH, and the equivalent distributed capacitance is 18.6 pF, which meets the requirements of obtaining a steep rising edge [24].

IV. Experimental Results and Discussion

To verify the effectiveness of the proposed power supply, an experimental platform is built in Fig. 13.

The DBD load used is a net plate structure; the barrier medium is 2 mm thick quartz glass close to the electrode plate, and the air gap distance is 2 mm. After being measured by the impedance analyzer (KEYSIGHT E4990A), the equivalent capacitance of DBD load before discharge is 46.2 pF. The high-voltage dc power supply is Dongwen high-voltage power supply DW-P102-100C50. The output dc voltage of this power supply is 0–1000 V; the maximum output current is 100 mA; the output pulse is measured by Tektronix P6015A high-voltage probe, and the load current is measured by Pearson broadband current sensor (model: 150, bandwidth: 40 Hz–20 MHz, sensitivity: 0.5 V/A). The waveform is recorded by Tektronix MDO4104C mixed domain oscilloscope (bandwidth: 1 GHz, maximum sampling frequency: 5 Gs/s). The image of the experimental platform is shown in Fig. 13.

Fig. 14 shows the maximum output voltage waveform of the pulse power supply in this article. The pulse amplitude is 5 kV and the pulsewidth is 300 ns, which meets the design requirements.

After testing the maximum output of the power supply, the amplitude adjustability and repetition frequency adjustability of the output voltage are tested, respectively.

A. Experimental Verification of the Adjustability of Pulse Amplitude

Fig. 15 shows the voltage waveforms of DBD load with dc charging voltage at a repetition frequency of 10 kHz. From the actual measurement, it can be seen that the load-side voltage waveform is a pulse waveform with oscillation decay, the pulsewidth is around 300 ns, and the rising edge is about 100 ns. At the same time, the output voltage can change continuously with the dc charging voltage and keep the load waveform without distortion, which is consistent with the analysis in Section II.

B. Experimental Verification of the Adjustability of Repetition Frequency

To verify the adjustable range of the output frequency of this power supply and to observe the changes in the discharge

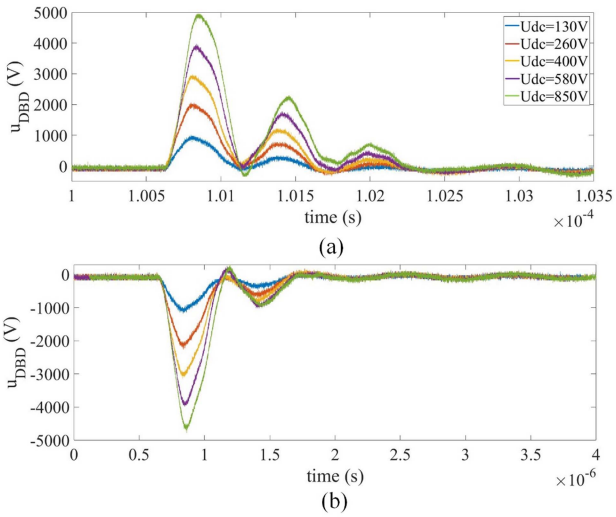

Fig. 15. Voltage waveforms on DBD load under different charging voltages. (a) Positive waveforms. (b) Negative waveforms.

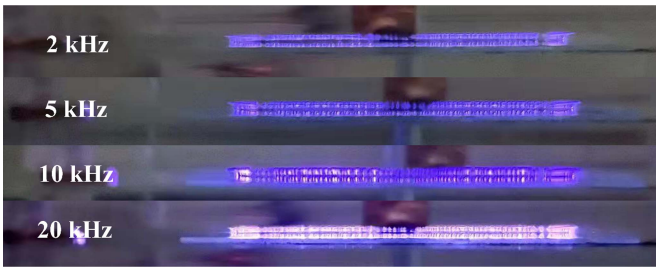

Fig. 16. Discharge images at different repetition frequencies with exposure times of 0.1 s.

situation under different repetition frequencies, the discharge images of the DBD load under the conditions of the output amplitude of 3 kV and repetition frequencies of 2 kHz, 5 kHz, 10 kHz, and 20 kHz are presented, respectively, in Fig. 16.

The DBD becomes more intense when the repetition frequency increases from 1 to 20 kHz. Especially when the repetition frequency is 20 kHz, the number of microdischarge channels becomes much more than that is 10 kHz. The results show that the proposed power supply can adjust the repetition frequency in the range of 0–20 kHz as required.

V. Conclusion

In this context, a bipolar compact ns pulse power supply with a maximum amplitude of 5 kV, a maximum repetition frequency of 20 kHz, a pulsewidth of 300 ns, and a rise time of 100 ns for DBD loads is proposed based on the BLTs structure combined with a pulse transformer. Based on the prototype, an experimental platform is built, and the DBD phenomenon under different repetition frequencies is preliminarily tested, and the following conclusions can be derived.

1) The characteristics of BLT and pulse transformer make the proposed topology adapt well to the DBD load. And it can maintain the ns voltage pulse without a parallel resistor, which will not cause extra energy loss. To some extent, it helps to improve the energy utilization of ns pulse topologies for driving DBD loads.
2) The transmission lines theory and Laplace transforms can well explain the principle of the proposed structure in this article. And it provides a good way to analyze pulsed power supplies, which consist of BLTs structure.
3) The output waveform of this power supply is stable and adjustable under different charging voltages and repetition frequencies, which provides a solution for designing a nanosecond pulse power supply, especially for driving the DBD loads.
4) The proposed power supply in this article has a modular structure, which improves reliability and scalability. The maximum output voltage can be adjusted by changing the pulse transformer modular and also can use repeat frequency technology in BLTs modular to improve the maximum frequency of the pulse.

References

[1] C. Zhang et al., "Surface treatment of polyethylene terephthalate films using DBD excited by repetitive unipolar nanosecond pulses in air at atmospheric pressure," *IEEE Trans. Plasma Sci.*, vol. 38, no. 6, pp. 1517–1526, Jun. 2010.
[2] N. Dumitrascu, I. Topala, and G. Popa, "Dielectric barrier discharge technique in improving the wettability and adhesion properties of polymer surfaces," *IEEE Trans. Plasma Sci.*, vol. 33, no. 5, pp. 1710–1714, Oct. 2005.
[3] Z. Fang, J. Lin, H. Yang, Y. Qiu, and E. Kuffel, "Polyethylene terephthalate surface modification by filamentary and homogeneous dielectric barrier discharges in air," *IEEE Trans. Plasma Sci.*, vol. 37, no. 5, pp. 659–667, May 2009.
[4] M. Blajan, A. Umeda, and K. Shimizu, "Surface treatment of glass by microplasma," *IEEE Trans. Ind. Appl.*, vol. 49, no. 2, pp. 714–720, Mar./Apr. 2013.
[5] V. I. Grinevich, E. Y. Kvitkova, N. A. Plastinina, and V. V. Rybkin, "Application of dielectric barrier discharge for waste water purification," *Plasma Chem. Plasma Process.*, vol. 31, no. 4, pp. 573–583, Aug. 2011.
[6] H. Wu, Z. Fang, and Y. Xu, "Degradation of aniline wastewater using dielectric barrier discharges at atmospheric pressure," *Plasma Sci. Technol.*, vol. 17, no. 3, pp. 228–234, Mar. 2015.
[7] P. Pourhadi Abkenar, H. Iman-Eini, M. H. Samimi, and M. Emaneini, "Design and implementation of ozone production power supply for the application of microbial purification of water," *IEEE Trans. Power Electron.*, vol. 35, no. 8, pp. 8215–8223, Aug. 2020.
[8] M. Amjad, Z. Salam, M. Facta, and S. Mekhilef, "Analysis and implementation of transformerless LCL resonant power supply for ozone generation," *IEEE Trans. Power Electron.*, vol. 28, no. 2, pp. 650–660, Feb. 2013.
[9] D. Florez, R. Diez, H. Piquet, and A. K. Hay Harb, "Square-shape current-mode supply for parametric control of the DBD excilamp power," *IEEE Trans. Ind. Electron.*, vol. 62, no. 3, pp. 1451–1460, Mar. 2015.
[10] Y. S. Jin and C. Cho, "Generation of plasma activated water by a hybrid plasma source," *IEEE Trans. Plasma Sci.*, vol. 47, no. 10, pp. 4588–4592, Oct. 2019.
[11] S. Bekeschus, A. Lin, A. Fridman, K. Wende, K.-D. Weltmann, and V. Miller, "A comparison of floating-electrode DBD and kinpen jet: Plasma parameters to achieve similar growth reduction in colon cancer cells under standardized conditions," *Plasma Chem. Plasma Process.*, vol. 38, no. 1, pp. 1–12, Jan. 2018.
[12] X. Bonnin, J. Brandelero, N. Videau, H. Piquet, and T. Meynard, "A high voltage high frequency resonant inverter for supplying DBD devices with short discharge current pulses," *IEEE Trans. Power Electron.*, vol. 29, no. 8, pp. 4261–4269, Aug. 2014.
[13] S. Hao, X. Liu, W. Li, Y. Deng, and X. He, "Energy compression of dielectric barrier discharge with third harmonic circulating current in current-fed parallel-series resonant converter," *IEEE Trans. Power Electron.*, vol. 31, no. 12, pp. 8528–8540, Dec. 2016.

[14] S. Jin, C. Zhang, Y. Peng, and Z. Fang, "Novel IPOx architecture for high-voltage microsecond pulse power supply using energy efficiency and stability model design method," *IEEE Trans. Power Electron.*, vol. 36, no. 9, pp. 10852–10865, Sep. 2021.
[15] C. Sanabria, D. Florez, H. Piquet, and R. Diez, "Sizing equations for a square voltage pulse power supply for dielectric barrier discharges," *IEEE Trans. Power Electron.*, vol. 37, no. 4, pp. 4374–4384, Apr. 2022.
[16] J. Rao, K. Liu, and J. Qiu, "A novel all solid-state sub-microsecond pulse generator for dielectric barrier discharges," *IEEE Trans. Plasma Sci.*, vol. 41, no. 3, pp. 564–569, Mar. 2013.
[17] T. Shao et al., "A compact repetitive unipolar nanosecond-pulse generator for dielectric barrier discharge application," *IEEE Trans. Plasma Sci.*, vol. 38, no. 7, pp. 1651–1655, Jul. 2010.
[18] Y. Mi, J. Wan, C. Bian, Y. Zhang, C. Yao, and C. Li, "A high-repetition-rate bipolar nanosecond pulse generator for dielectric barrier discharge based on a magnetic pulse compression system," *IEEE Trans. Plasma Sci.*, vol. 46, no. 7, pp. 2582–2590, Jul. 2018.
[19] S. K. Rai, A. K. Dhakar, and U. N. Pal, "A compact nanosecond pulse generator for DBD tube characterization," *Rev. Sci. Instrum.*, vol. 89, no. 3, Mar. 2018, Art. no. 033505.
[20] A. K. Dhakar, S. K. Rai, V. K. Saini, S. K. Sharma, and U. N. Pal, "Simplified high-voltage short-pulse power modulator for DBD plasma application," *IEEE Trans. Plasma Sci.*, vol. 49, no. 4, pp. 1422–1427, Apr. 2021.
[21] P. Seri et al., "Influence of the voltage waveform's shape and on-time duration on the dissolved ozone produced by a DBD bubble reactor," *Plasma Sources Sci. Technol.*, vol. 28, no. 3, Mar. 2019, Art. no. 035001.
[22] J. M. Williamson, D. D. Trump, P. Bletzinger, and B. N. Ganguly, "Comparison of high-voltage AC and pulsed operation of a surface dielectric barrier discharge," *J. Phys. D, Appl. Phys.*, vol. 39, no. 20, pp. 4400–4406, 2006.
[23] M. Gundersen, P. T. Vernier, S. B. Cronin, and S. Kerketta, "A review of diverse academic research in nanosecond pulsed power and plasma science," *IEEE Trans. Plasma Sci.*, vol. 48, no. 4, pp. 742–748, Apr. 2020, doi: 10.1109/tps.2020.2972934.
[24] Y. Zhou et al., "Fast-rise-time trigger source based on solid-state switch and pulse transformer for triggered vacuum switch," *IEEE Trans. Dielectr. Elect. Insul.*, vol. 24, no. 4, pp. 2105–2114, Sep. 2017.
[25] Y. Wang, L. Tong, K. Liu, and Y. Huang, "Repetitive high-voltage pulse modulator using bipolar marx generator combined with pulse transformer," *IEEE Trans. Plasma Sci.*, vol. 46, no. 10, pp. 3340–3347, Oct. 2018.
[26] E. Panousis et al., "Analysis of dielectric barrier discharges under unipolar and bipolar pulsed excitation," *IEEE Trans. Dielectr. Elect. Insul.*, vol. 16, no. 3, pp. 734–741, Jun. 2009.
[27] D. H. Barnett et al., "Optically isolated, 2 kHz repetition rate, 4 kV solid-state pulse trigger generator," *Rev. Sci. Instrum.*, vol. 86, no. 3, 2015, Art. no. 034702.
[28] D. Aguglia, J.-M. Cravero, R. Rebeschini, S. Iovieno, and C. Russo, "Design solutions for compact high current pulse transformers for particle accelerators' magnets powering," in *Proc. 17th Eur. Conf. Power Electron. Appl.*, 2015, pp. 1–8.
[29] Y. Wang, M. Li, K. Li, and G. Zhang, "Optimal design and experimental study of pulse transformers with fast rise time and large pulse duration," *IEEE Trans. Plasma Sci.*, vol. 42, no. 2, pp. 300–306, Feb. 2014.
[30] D. Aguglia, "Pulse transformer design for magnet powering in particle accelerators," in *Proc. 15th Eur. Conf. Power Electron. Appl.*, 2013, pp. 1–9.
[31] L. Jinliang, Z. Jiande, L. Yongzhong, L. Jijian, and F. Jiahuai, "High voltage pulse transformer for PFL charging," *High Power Laser Part. Beams*, vol. 15, no. 4, pp. 394–396, 2003.

Hao Gui was born in Mianyang, China, in 1999. He received the B.S. degree in 2021 from the College of Engineering and Technology, Southwest University, Chongqing, China, where he is currently working toward the master's degree with the College of Engineering and Technology.

His research area is pulse power technology.

Zhongyong Zhao (Member, IEEE) was born in Guangyuan, China. He received the B.S. and Ph.D. degrees in electrical engineering from Chongqing University, Chongqing, China, in 2011 and 2017, respectively.

He received a scholarship from China Scholarship Council to enable him to attend a joint-training Ph.D. program with Curtin University, Perth, WA, USA, in 2015 and 2016. He is currently an Associate Professor with the College of Engineering and Technology, Southwest University, Chongqing, China. His areas of research include condition monitoring and fault diagnosing for HV apparatus and artificial intelligence.

Qing Shi was born in Sichuan, China, in 1999. She received the B.S. degree from the College of Mechanical and Electrical Engineering, Sichuan Agricultural University, Sichuan, China, in 2021. She is currently working toward the master's degree with the College of Engineering and Technology, Southwest University, Chongqing, China.

She is mainly engaged in research related to triboelectric nanogenerators and their self-powered applications.

Xin Liu (Student Member, IEEE) was born in Guangan, China, on August 26, 1992. He received the B.S. degree in electrical engineering from the University of Electronic Science and Technology of China, Chengdu, China, in 2014, and the M.S. degree in electrical engineering in 2017 from Chongqing University, Chongqing, China, where he is currently working toward the Ph.D. degree in electrical engineering.

His areas of research include power transformers measurement technology, planar transformer, and pulse transformer design for high-voltage pulse generator.

Chenguo Yao (Member, IEEE) was born in Nanchong, China. He received the B.S., M.S., and Ph.D. degrees in electrical engineering from Chongqing University, Chongqing, China, in 1997, 2000, and 2003, respectively.

In 2007, he became a Professor with the College of Electrical Engineering, Chongqing University. His current research interests include pulse power technology and its application in biomedical engineering, online monitoring of insulation condition, and insulation fault diagnosis for high-voltage apparatus.